Robotica (2005) volume 23, pp. 109–122. © 2005 Cambridge University Press
DOI: 10.1017/S0263574704000402 Printed in the United Kingdom

# Optimal design of a micro parallel positioning platform. Part II: Real machine design

Kun-Ku Oh, Xin-Jun Liu, Deuk Soo Kang and Jongwon Kim*

*School of Mechanical and Aerospace Engineering, Seoul National University, Seoul 151-744 (Republic of Korea)*

(Received in Final Form: March 8, 2004)

**SUMMARY**

In part I of this paper (previous issue of *Robotica*) a dual stage system with the coarse and fine actuators is adopted to achieve sub-micron accuracy with a large working space for the proposed new three degree-of-freedom (DOF) miniaturized micro parallel mechanism with high mobility and one type of the architecture with vertical actuator locations in all three legs (C-VV type) among six possible coarse actuator architectures is selected for the coarse actuator architecture.

In this part of the paper, an optimal kinematic parameter set is determined for the selected coarse actuator architecture. To determine this set, the design tool of the physical model of the solution space (PMSS) and the evaluation of the conditioning index (*CI*) and global mobility conditioning index (*GMCI*) are used. The basic size of the micro parallel mechanism is 45.0 mm × 22.5 mm × 22.9 mm with 100° mobility, the workspace 5.0 mm ($y$-axis) × 5.0 mm ($z$-axis), and sub-micron resolution. After finishing the design of the main coarse actuator architecture, one architecture among six possible fine actuator architectures is selected to achieve sub-micron positioning accuracy based on the requirements of the continuous fine motion and smaller platform resolution. The selected coarse-and-fine actuator combination is used for the micro positioning platform for laser-machining application.

KEYWORDS: Parallel mechanism; Micro positioning platform; Dual stage system; Design optimization

## 1. INTRODUCTION

Determination of the architecture and size of a mechanism is an important issue in mechanism design. The performances of parallel mechanisms, especially, depend heavily on the kinematic parameters (link lengths). Therefore, the kinematic parameters most suitable for the task must be designed with respect to performances (e.g. workspace and condition number). Unfortunately, any change that improves one performance will usually deteriorate another. This trade-off occurs with almost every design and this inevitably generates the problem of design optimization.

The classical methods of design optimization, such as iterative methods, suffer from difficulties in dealing with this problem.[1,2] Firstly, optimization problems can take many iterations to converge and can be sensitive to numerical problems such as truncation and round-off error in the calculation. Secondly, most optimization problems depend on the initial guesses, and identification of the global minimum is not guaranteed. Therefore, the relation between the design parameters and objective function is difficult to know, thus making it hard to obtain the most optimal design parameters of the mechanism.

The link lengths of mechanisms can be measured by various units and can be changed between zero and infinity, which means that the links can be very long or short. Therefore, it is difficult to investigate the relations between performance criteria and link lengths of all mechanisms. So it is important to develop a useful design tool that can express the relations between performance criteria and link lengths. A design tool, the physical model of the solution space (PMSS),[3] which is proposed by one of the authors (Xin-Jun Liu), is a useful tool that converts the physical sizes of mechanisms to non-dimensional link lengths and embodies them in a finite solution space. The relations between the performance criteria and link lengths of all mechanisms can be plotted in the physical model of the solution space, and then the performance distributions within the PMSS are obtained. Based on the performance distributions, we can select an optimal parameter set for the mechanism.

On the other hand, to manufacture, assemble, or manipulate micro three-dimensional precise components, a positioning device with sub-micron accuracy and high mobility (rotational capability) over a large working space is needed. Common method to achieve sub-micron accuracy is to use the stage with piezoelectric fine actuators and wire-EDM-cut flexures.[4] However, these fine actuators have usually less than 100 microns of motion range and show no or little spatial rotational capability. One of the practical methods to achieve sub-micron accuracy with a large working space is to use the dual stage system with the coarse and fine actuators. The coarse actuator offers a large working space and actuation powers while the fine actuator enables high resolution of motion.

In part I of this paper (previous issue of *Robotica*) the dual stage system with the coarse and fine actuators is adopted to achieve sub-micron accuracy with a large working space for the proposed new three degree-of-freedom (DOF) miniaturized micro parallel mechanism with high mobility. One type of the architecture with vertical actuator locations in all three legs (C-VV type) among six possible coarse actuator architectures is selected for the coarse actuator architecture.

* Corresponding author. E-mail address: jongkim@snu.ac.kr

https://doi.org/10.1017/S0263574704000402 Published online by Cambridge University Press

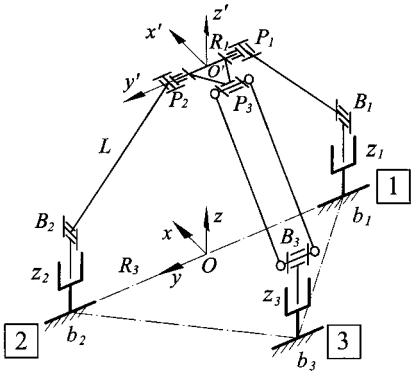


Fig. 1. The selected VV type for the coarse actuator architecture.

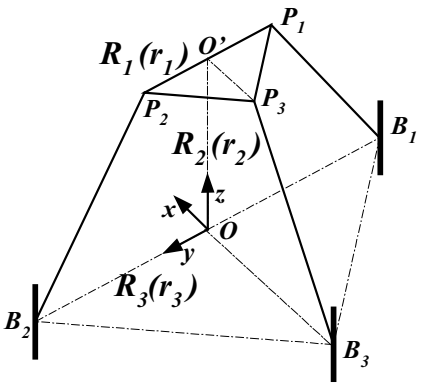


Fig. 2. Three parameters to establish the physical model of the solution space.

In this part of the paper the design tool, the physical model of the solution space (PMSS), is applied to the optimal design of the selected coarse actuator architecture. For the performance criteria, the combination of the conditioning index (*CI*) and global mobility conditioning index (*GMCI*) based on the condition number is used. The target specifications for the overall size and working space of the micro-parallel mechanism are less than 50 mm × 50 mm × 50 mm and more than $\phi$5 mm × height 5 mm with 100° mobility, respectively. Here, the different design aspects in the micro machine design such as previous consideration of available coarse actuators before the real design process, manufacturability, and easy assembly are addressed. After finishing the design of the main coarse actuator architecture, one fine actuator architecture among six possible fine actuator architectures is selected to achieve sub-micron positioning accuracy meeting the requirements of the continuous fine motion and smaller platform resolution. Finally, the design application for a micro positioning platform based on the selected coarse-and-fine actuator combination is presented.

## 2. OPTIMUM DESIGN OF THE MECHANISM

In part I of this paper, the C-VV type, as shown in Fig. 1, is selected for the coarse actuator architecture of the micro parallel mechanism with the dual stage system. This section is to determine the appropriate kinematic parameters for the selected VV type coarse actuator architecture with respect to desired performance such as workspace, accuracy, and mobility.

### *2.1. Physical model of the solution space*

For our parallel mechanism, there are three kinematic parameters, which are $R_1$ (the radius of the moving platform), $L$ (the length for each of the three links) and $R_3$ (the radius of the base plate) as shown in Fig. 1. To facilitate the presentation, an additional parameter $R_2$, which is the vertical distance between the origin of the moving platform and the 1st or 2nd base joint (that is, the distance between lines $P_1P_2$ and $B_1B_2$ in Fig. 2) at the home position $O'$ (0,0,0), is introduced into the kinematic parameters as shown in Fig. 2. There is a relation of $L = \sqrt{(R_3 - R_1)^2 + R_2^2}$ between these kinematic parameters.

Because each of three parameters $R_1$, $R_2$, and $R_3$ can vary from zero to infinity, it is difficult to study the performances of all these mechanisms with these parameters. Therefore, it is important to find a tool that can express all mechanisms with these parameter sets in a finite design space characterized by kinematic parameters. We will determine the best ratio between the kinematic parameters of the 3-DOF parallel mechanism based on such a design tool, the physical model of the solution space (PMSS),[3] which was proposed by one of the authors (Xin-Jun Liu). The relationships between performance criteria and kinematic parameters can be plotted in the PMSS, and then the performance distributions within the PMSS will be obtained. Based on the performance distributions, we can select an optimal parameter set for the mechanism.

In the PMSS, the required performances of all the possible kinematic parameters can be represented by means of the non-dimensional parameters of a finite space, from which we can select the optimal parameters. For this reason, we must eliminate the physical link size of the kinematic parameters by introducing the scaling factor $D$, which is defined as

$$D = \frac{R_1 + R_2 + R_3}{3} \tag{1}$$

The kinematic parameters $R_1$, $R_2$, and $R_3$ divided by $D$ are defined as three non-dimensional parameters $r_1, r_2$ and $r_3$, respectively, i.e.,

$$r_1 = \frac{R_1}{D}, \quad r_2 = \frac{R_2}{D}, \quad r_3 = \frac{R_3}{D} \tag{2}$$

Hence, we can obtain the PMSS for the mechanism, such as

$$r_1 + r_2 + r_3 = 3 \quad \text{where } 0 < r_1, r_2, r_3 < 3, \quad \text{and } r_1 \le r_3 \tag{3}$$

This process reduces the three-dimensional parameter space to a two-dimensional one, which a designer can conveniently use to analyze the performances of the mechanism. For convenience, we transformed $r_1, r_2$ and $r_3$ into two orthogonal coordinates $s$ and $t$ by

$$s = \frac{2}{\sqrt{3}} r_1 + \frac{1}{\sqrt{3}} r_2, \quad t = r_2 \tag{4}$$

https://doi.org/10.1017/S0263574704000402 Published online by Cambridge University Press

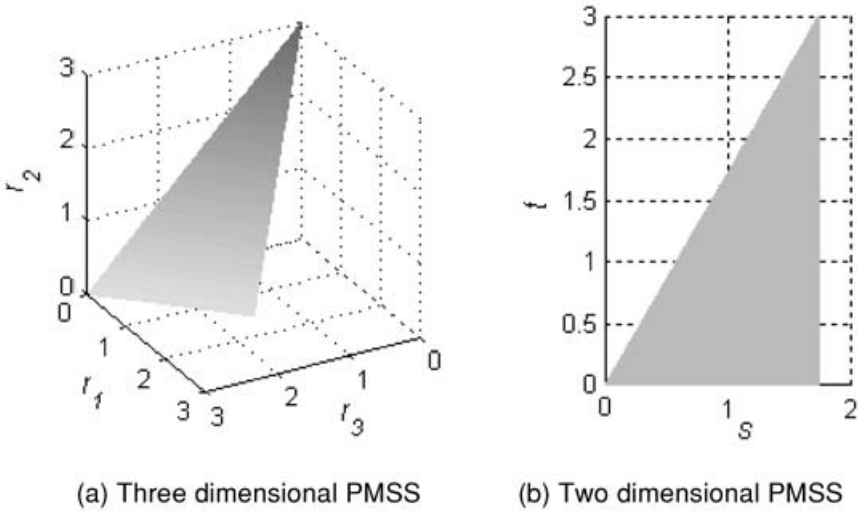


Fig. 3. Graphic representation of the physical model of the solution space (PMSS).

Inversely, we can transform coordinates $s$ and $t$ into $r_1$, $r_2$ and $r_3$ by means of

$$r_1 = \frac{\sqrt{3}s - t}{2}, \quad r_2 = t, \quad r_3 = 3 - r_1 - r_2 \tag{5}$$

Fig. 3 shows the graph for the PMSS of Eq. (3) and its two-dimensional representation of Eq. (4).

### *2.2. Design optimization*

In the VV type coarse actuator architecture, the mechanism has vertical ($z$ directional) actuator locations in all three legs. Therefore, if we know the whole characteristics of our mechanism along the $y$ directional workspace, the same characteristics can be applied to all the other values of the $z$ directional workspace. The $CI$ distribution of the VV type in Fig. 9(a) of part I confirms this result, where the $CI$ values are same along the z coordinates of the platform. For the $y$ directional workspace of a mechanism within the PMSS, we introduce the non-dimensional working space of $y \in [-\frac{r_1}{2}, +\frac{r_1}{2}]$. So it is enough to evaluate various parameter sets within the PMSS in the range of the non-dimensional $y$ directional working space, $y \in [-\frac{r_1}{2}, +\frac{r_1}{2}]$, for a specific $z$ value (here, we will use $z = 0$.)

The objective function to determine the optimal parameters is as follows.

$$\underset{r_1, r_2, r_3}{Max} \left[ \frac{CI(y=0, \phi=\phi_m) + GMCI(y=0, \phi=[\phi_m - 50^\circ, \phi_m + 50^\circ])}{2} \right]$$

$$\text{subject to} \begin{cases} \text{LM}\left(y = \pm\dfrac{r_1}{2}\right) > 100^\circ \\ CI\left(y = \pm\dfrac{r_1}{2}, \phi = \phi_m \pm 50^\circ\right) > 0.1 \\ \dfrac{R_3}{Z_{c3}} = \dfrac{r_3}{z_{c3}} \geq \dfrac{22.5}{17} = 1.3235 \\ \dfrac{R_1}{Z_{c3}} = \dfrac{r_1}{z_{c3}} \geq \dfrac{5}{17} = 0.2941 \end{cases} \tag{6}$$

where $CI(y=0, \phi=\phi_m)$ and $GMCI(y=0, \phi=[\phi_m - 50^\circ, \phi_m + 50^\circ])$ represent the conditioning index ($CI$) of the home position ($O'$ (0,0,0), $\phi = \phi_m$) and the global mobility conditioning index ($GMCI$) of $O'$ (0,0,0) for the 100° tilting angle, respectively, as the same with the definitions in part I. Here $\phi_m$ is the middle angle of the local mobility of the position, the angle which represents 100° tilting range with the interval $[\phi_m - 50^\circ, \phi_m + 50^\circ]$. The distribution of the middle angle $\phi_m$ is shown in Fig. 4. The distribution of the $(CI + GMCI)/2$ is shown in Fig. 5 for the objective function of Eq. (6) within the PMSS.

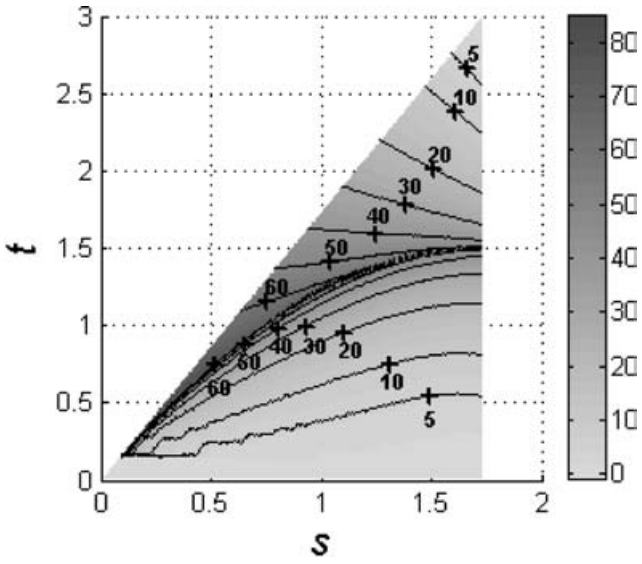

Fig. 4. Middle angle $\phi_m(^\circ)$ distribution within the PMSS.

The first constraint, $LM(y = \pm\frac{r_1}{2}) > 100^\circ$, is given to consider the area with the mobility of more than 100°. Here, $y = \pm\frac{r_1}{2}$ is selected for the local mobility evaluation because these positions have the lowest $CI$ values along the $y$ directional workspace as shown in the $CI$ distribution of the VV type of Fig. 9(a) in part I. The distribution of $LM$ within the PMSS is shown in Fig. 6(a).

Although the value of the objective function may be large, it is possible to have singularities in some area within the workspace. This situation can be avoided by adding another minimum $CI$ constraint in the objective function such as

https://doi.org/10.1017/S0263574704000402 Published online by Cambridge University Press

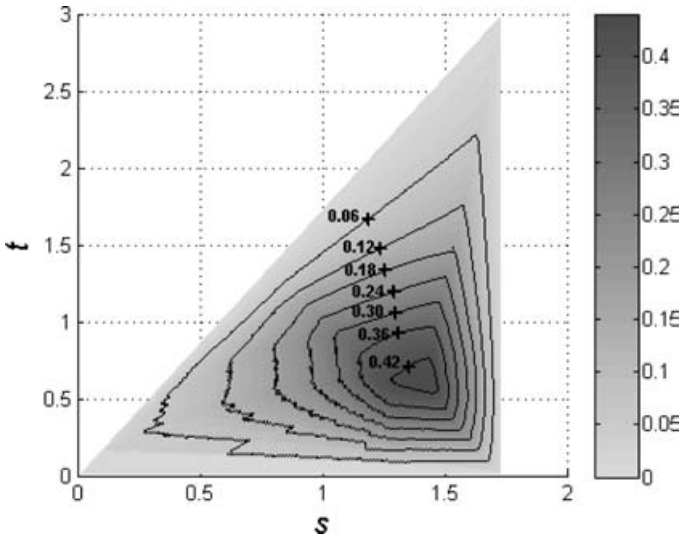


Fig. 5. Distribution of $(CI + GMCI)/2$ within the PMSS.

$CI(y = \pm\frac{r_1}{2}, \phi = \phi_m \pm 50^\circ) > 0.1$, because $CI$ is considered as a measure of the kinematic accuracy and the proximity to singularity of a mechanism as discussed in section 4 of part I. We select the $CI(y = \pm\frac{r_1}{2}, \phi = \phi_m \pm 50^\circ) > 0.1$, where the mechanism has worst $CI$ values in poses $(y = \pm\frac{r_1}{2}, \phi = \phi_m \pm 50^\circ)$ as shown in Fig. 9 of Part I, in order to reduce the search region on the PMSS (Physical model of the solution space) and avoid the singular configuration. The selection of $CI > 0.1$ was based on the trial and error from the minimum $CI$ distribution of Fig. 6(b). In singular configuration $CI = 0$, so it is better to have larger minimum $CI$ to locate the mechanism far from singularity. For this purpose if we set the minimum $CI$ too high, we cannot find the optimal parameter set that satisfies all the constraints, but on the other hand, if we set the minimum $CI$ too low, the selected optimal parameter set is near the singular position around the moving platform poses of $(y = \pm\frac{r_1}{2}, \phi = \phi_m \pm 50^\circ)$ although the value of the objective function $(CI + GMCI)/2$ is large. The distribution of the minimum $CI$ within the PMSS is shown in Fig. 6(b).

To develop a miniaturized micro mechanism with high mobility, three miniaturized actuators should be located within the target size of the mechanism (less than 50 mm × 50 mm × 50 mm), and the third actuator, especially, should have a large stroke to achieve the mobility of more than 100°. Therefore, we need precise, miniaturized actuators with small size, large stroke and high resolution, which are very hard to find in the industry. In this sense, we need to select available actuators before determining kinematic parameters contrary to the conventional design process where we first determine design parameters and then select proper actuators.

Based on this knowledge, at first, we selected commercially available suitable miniaturized actuators for the mechanism as shown in Fig. 7, which also shows the recommended actuator architecture for the micro parallel mechanism. For the 1st and 2nd legs, the linear actuator with a stroke of

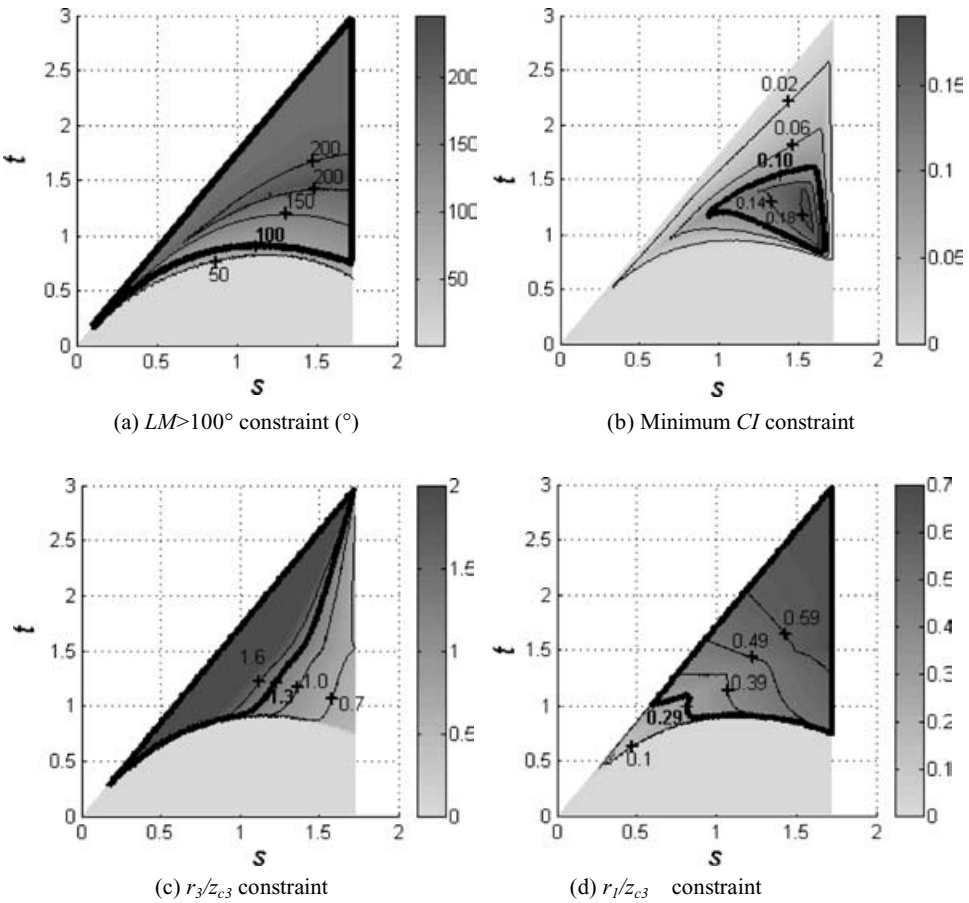


(a) $LM$>100° constraint (°)

(b) Minimum $CI$ constraint

(c) $r_3/z_{c3}$ constraint

(d) $r_1/z_{c3}$ constraint

Fig. 6. Constraint representations in the PMSS.

https://doi.org/10.1017/S0263574704000402 Published online by Cambridge University Press

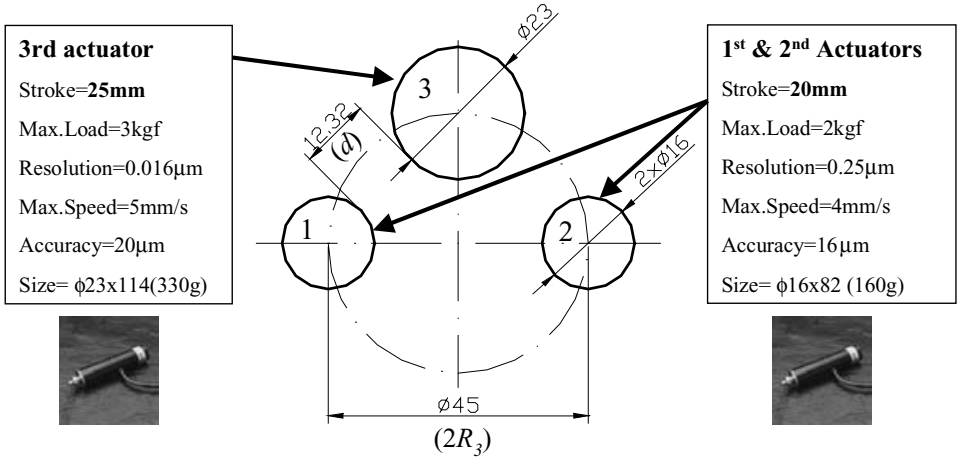


Fig. 7. Linear actuators to be used and its configuration (top view) unit:mm.

20.0 mm and 16.0 mm in outer diameter will be used. For the 3rd leg, the linear actuator with a stroke of 25.0 mm and 23.0 mm in outer diameter will be used. There should be enough space between the $Z_{c1}/Z_{c2}$ and $Z_{c3}$ actuators (e.g. more than 10 mm) to allow the fixture design and easy assembly for each actuator. This space ($d$) and $R_3$ are related by $d\,(\text{mm}) = \sqrt{2}R_3 - \frac{16}{2} - \frac{23}{2}$ from the configuration of Fig. 7, in which if $d > 10$ mm, $R_3$ should be larger than 20.86 mm. For convenience, $R_3 = 22.5$ mm is chosen, where $d$ is 12.32 mm as shown in Fig. 7.

Thus, to implement the actuator architecture in Fig. 7 and achieve the target specification for working space ($\phi 5$ mm × height 5 mm with 100° mobility), we need to consider the minimum $R_1$ and $R_3$ of the real mechanism depending on the stroke of $Z_{c3}$ actuator (the 3rd actuator). For the stroke of the $Z_{c3}$ actuator, we consider the height of workspace (5 mm) and allowance (3 mm) for the safe operation. So, the available stroke for the $Z_{c3}$ actuator with 25 mm stroke at the design stage will be 17.0 mm (= 25.0–5.0–3.0). Hence, the constraint between the minimum $R_3$ and available $Z_{c3}$ stroke will be $\frac{R_3}{Z_{c3}} = \frac{r_3}{z_{c3}} \geq \frac{22.5}{17}$ where $z_{c3}$ represents $Z_{c3}$ divided by $D$ as a non-dimensional stroke of the $Z_{c3}$ actuator. The distribution of $r_3/z_{c3}$ within the PMSS is shown in Fig. 6(c).

For the minimum $R_1$, we need to satisfy more than 5 mm in the $y$ directional working space of $y \in [-\frac{r_1}{2}, +\frac{r_1}{2}]$, therefore, the constraint between the minimum $R_1$ and available $Z_{c3}$ stroke will be $\frac{R_1}{Z_{c3}} = \frac{r_1}{z_{c3}} \geq \frac{5}{17}$. The distribution of $r_1/z_{c3}$ within the PMSS is shown in Fig. 6(d).

The last two constraints in the objective function of Eq. (6) represent these additional constraints of the minimum $R_1$ and $R_3$ of the real mechanism depending on the stroke of $Z_{c3}$ actuator (the 3rd actuator). Hence we recognize the different design aspects in the micro machine design, such as previous consideration of available actuators before the real design process, manufacturability, and easy assembly.

The constraints in Eq. (6) reduce the possible design parameter space in the PMSS. Figure 6(a), (b), (c) and (d) show the areas that satisfy the $LM > 100°$ constraint, the minimum $CI$ constraint, the minimum $R_3$ constraint, and the minimum $R_1$ constraint within the PMSS, respectively, where satisfying areas are represented by closed thick lines. In Fig. 6(a) and (b), the lower area of the PMSS is near zero because the mechanism with the parameter sets of the area become singular and has little mobility when $y = \pm\frac{r_1}{2}$. In Fig. 6(c) and (d) the area with the local mobility less than 100°, the lower area of the PMSS, is excluded in the evaluation and represented by zero because $z_{c3}$ stroke should be calculated for the 100° tilting range, and the stroke cannot be evaluated in the area with the local mobility less than 100°.

Figure 8(a) shows $(CI + GMCI)/2$ distribution for the objective function of Eq. (6) within the PMSS considering the combination of all these constraints of Fig. 6, where the common intersection area of all constraints is represented by the closed thick line. This intersection area is enlarged in Fig. 8(b) with the display of $(CI + GMCI)/2$ values. From the reduced design parameter space in the PMSS of Fig. 8(b) satisfying all constraints, one can select the optimal combination of $s$ and $t$. The maximum $(CI + GMCI)/2$ is located in the lower middle area in Fig. 8(b).

Thus, we obtain the optimal set of kinematic parameters $s = 1.18$, $t = 1.15$ when $(CI + GMCI)/2 = 0.23$ from Fig. 8(b). These parameters correspond to $r_1 = 0.45$, $r_2 = 1.15$, $r_3 = 1.40$ and $\ell = 1.49$ by Eq. (5). For these parameters, $LM = 142.43°$ and $\phi_m = 27.81°$. To implement this parameter set to the real mechanism, the scaling factor $D$ and related enlarged parameters that can realize the real mechanism architecture of Fig. 7 are calculated in the third column of Table I.

The $CI$ distribution of the optimal parameter set is shown in Fig. 9(a). As shown in Fig. 9(a), if we shift the middle angle $\phi_m$ to the right, as long as the $Z_{c3}$ stroke is allowed, the $CI$ distribution can be improved. For the stroke of the $Z_{c3}$ actuator, we considered the height (5 mm) of the workspace and allowance (3 mm) for the safe operation. If we reduce the allowance from 3 mm to 1 mm, the available stroke for the $Z_3$ actuator with 25.0 mm stroke will be enlarged form 17.0 mm to 19.0 mm (= 25-5-1). By using this, we can shift the middle angle $\phi_m = 27.81°$ to the new tilting angle $\phi_o = 37.15°$ as shown in Fig. 9(b). By this shifting, the new $(CI + GMCI)/2$ value becomes from 0.23 to 0.25 (8.7% improvement), and the minimum $CI$ also improved from 0.10 to 0.13 (30% improvement). These results are summarized in the fourth column of Table I.

https://doi.org/10.1017/S0263574704000402 Published online by Cambridge University Press

Table I. Optimal design parameter set and its enlarged and shifted parameter sets for realization.

| Items | Design parameters | Enlarged ($R_3 = 22.5$) | After shifting ($R_3 = 22.5$) |
|---|---|---|---|
| $D$ (scaling factor) | | 16.11 | 16.11 |
| $r_1$ | 0.45 | $R_1 = 7.32$ mm | $R_1 = 7.32$ mm |
| $r_2$ | 1.15 | $R_2 = 18.50$ mm | $R_2 = 18.50$ mm |
| $r_3$ | 1.40 | $R_3 = 22.50$ mm | $R_3 = 22.50$ mm |
| $\ell$ | 1.49 | $L = 23.93$ mm | $L = 23.93$ mm |
| $\phi_m$ | 27.81° | 27.81° | $\phi_o = 37.15°$ |
| *Local Mobility* (*LM*) | 142.43° | 142.43° | 142.43° |
| $(CI + GMCI)/2$ | 0.23 | 0.23 | 0.25 |
| Min($CI$) | 0.10 | 0.10 | 0.13 |
| Required $z_{c3}$ stroke | 1.06 | $Z_{c3} = 17.00$ mm | $Z_{c3} = 18.96$ mm |
| Required $z_{c1}$ & $z_{c2}$ strokes | 0.39 | $Z_{c1}$ &$Z_{c2} = 6.22$ mm | $Z_{c1}$ & $Z_{c2} = 6.22$ mm |

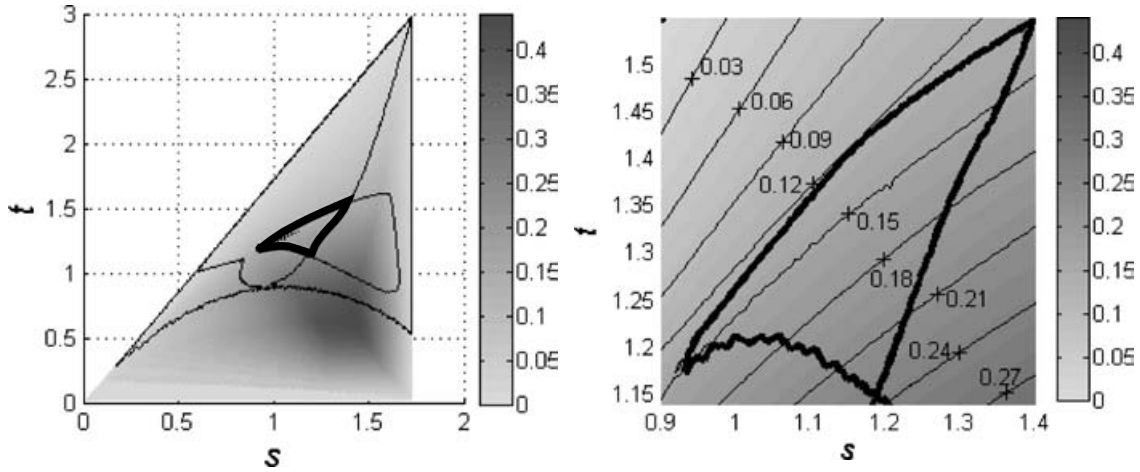


(a) Intersection of all constraints within PMSS (b) Enlarged view for the intersection area

Fig. 8. Distribution of $(CI + GMCI)/2$ considering the intersection of all constraints within the PMSS.

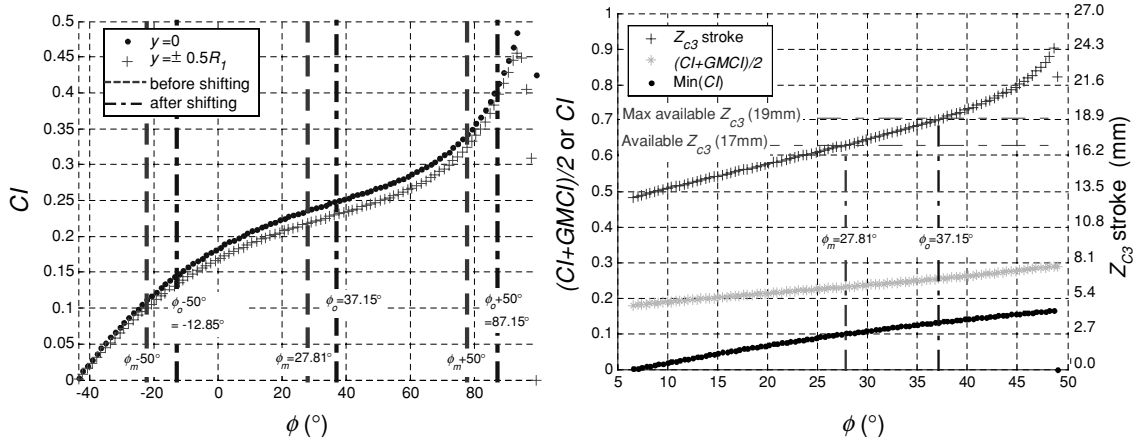


(a) $CI$ distributions for optimal parameter set (b) shifting considering $Z_{c3}$ stroke for better $CI$

Fig. 9. $CI$ distribution and shifting.

The final optimal kinematic parameter set and its 100° mobility sketch at $O'(0,0,0)$ after shifting are shown in Fig. 10, where the basic size of the micro parallel mechanism is 45.0 mm × 22.5 mm × 22.9 mm except the size of actuators. If we consider the height (5 mm) of the workspace, which was ignored in the design process, the real required $Z_{c3}$ stroke is 23.96 mm (18.96 + 5.0) for the working space of $y \in [-\frac{R_1}{2}, +\frac{R_1}{2}]$ and $z \in [0, 5]$ with 100° mobility. For the $Z_{c1}$ and $Z_{c2}$ actuators the required strokes are 11.20 mm (6.22 + 5.0) in the same way, but this is not affected by shifting the middle angle $\phi_m$, which is only related to the movement of $Z_{c3}$ actuator. We can confirm that the selected

https://doi.org/10.1017/S0263574704000402 Published online by Cambridge University Press

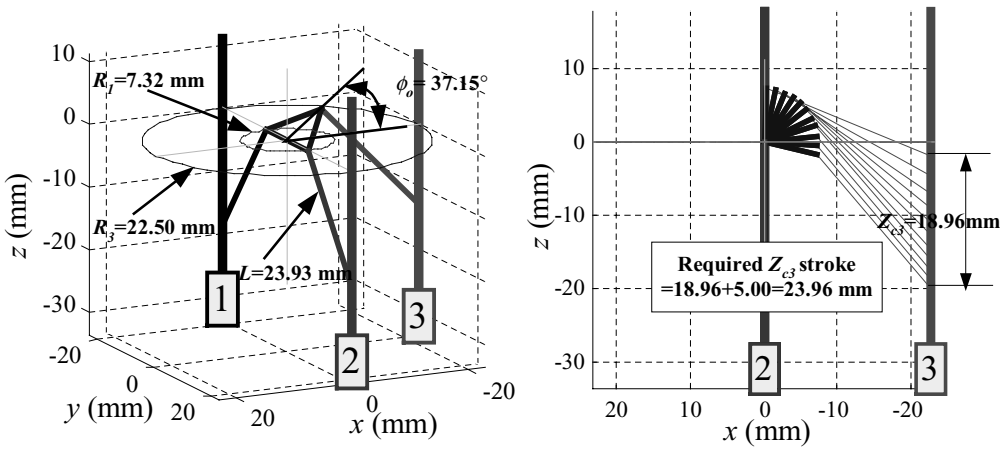


(a) Optimal parameter set (b) 100° mobility sketch at $O'(0,0,0)$

Fig. 10. Selected final optimal parameter set and its mobility sketch.

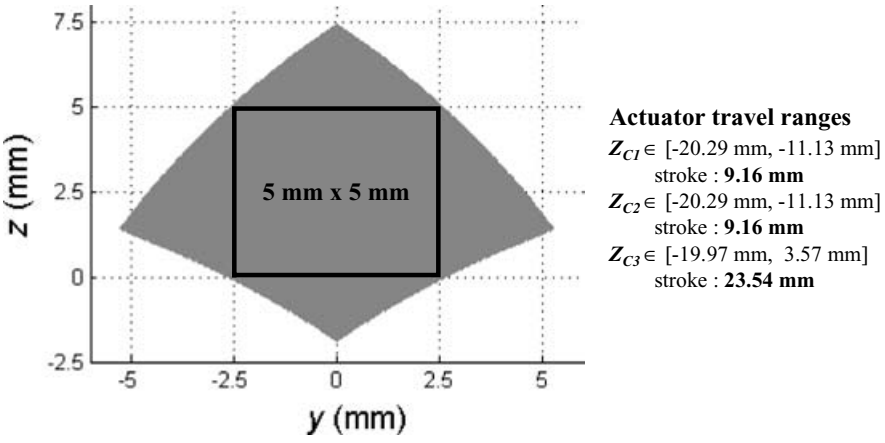


Fig. 11. Workspace of the miniaturized micro parallel mechanism.

actuators are appropriate from the viewpoint of the required strokes because the strokes for the $Z_{c1}/Z_{c2}$ and $Z_{c3}$ actuators are 20.0 mm and 25.0 mm, respectively, as shown in Fig. 7.

*2.3. Analysis on the optimal kinematic parameter set*

Target working space for the mechanism is $\phi$5 mm × height 5 mm with 100° mobility as mentioned in the introduction. The travel ranges for the three coarse actuators can be calculated by the inverse kinematics of section 3.1 in part I as given in Eq. (7) for the workspace of 5.0 mm ($y$-axis) × 5.0 mm ($z$-axis). The workspace for the selected actuators and optimal parameters is shown in Fig. 11.

$$Z_{c1}, Z_{c2} \in [-20.29\,\text{mm}, -11.13\,\text{mm}] \quad \text{and}$$
$$Z_{c3} \in [-19.97\,\text{mm}, 3.57\,\text{mm}] \tag{7}$$

Figure 12 displays the local mobility distribution within workspace, where we can verify the mobility of more than 100° within workspace. Note that we consider not only the kinematic compatibility but also the actuator travel range of Eq. (7) when evaluating this local mobility distribution. For example, when we only considered the kinematic compatibility, the local mobility at $O'(0,0,0)$ was 145.21° as shown in Fig. 6(a) in part I. This value can be called as the maximum local mobility at $O'(0,0,0)$ because the limitless actuator travel range is assumed in this calculation. However, when we consider the actuator travel range of Eq. (7), the local mobility at $O'(0,0,0)$ is reduced to 111.88° as shown in Fig. 13, where it is confirmed that this reduced local mobility range is the middle part of the maximum local mobility, which is far away from singularities.

Figure 14 and Fig. 9(a) show the *CI* distribution within the workspace where we can confirm that the *CI* values are more than 0.13 in the whole workspace, thus there is no singularity within the workspace.

## 3. SELECTION OF THE FINE ACTUATOR ARCHITECTURE

We selected the VV type for the coarse actuator architecture and determined its optimal parameters set. The selection problem of the fine actuator architecture will be discussed in this section. As shown in Fig. 15, there are six possible architectures with fine actuators.

https://doi.org/10.1017/S0263574704000402 Published online by Cambridge University Press

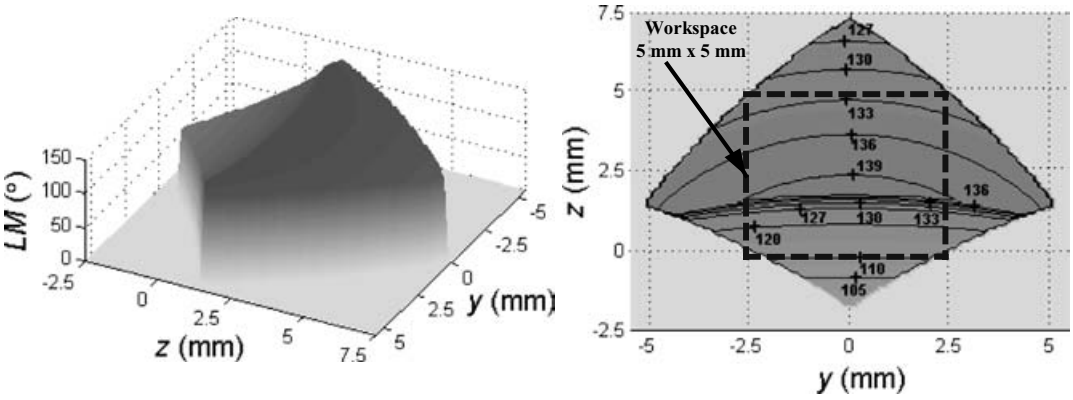


(a) Local mobility distribution (3D) (b) Top view of the local mobility

Fig. 12. Local Mobility (*LM*) distribution within the workspace.

Y. Takeda et al.[5] used the stroke and resolution of fine actuator to show the infinitesimal displacement characteristics for four possible coarse-and-fine actuator architectures. He selected one architecture, but the selection procedure was not clear. In this work we will show the detail procedure and selected one architecture based on the numerical comparison.

Two criteria for evaluating each fine actuator architecture will be used: First, to achieve the continuous fine motion requirement, the strokes of the fine actuators should be larger than the resolutions of the coarse actuators, and second, to develop a mechanism having more accuracy, a smaller platform resolution is desirable. For this purpose, the equations for the Jacobian relations of the coarse and fine actuator combinations, the required fine actuator strokes in terms of the coarse actuator resolutions, and the platform resolutions in terms of the fine actuator resolutions are derived in Table II, where $\Delta \boldsymbol{p}$, $\Delta \boldsymbol{\rho}_C$ and $\Delta \boldsymbol{\rho}_F$ denote infinitesimal displacement vectors of the movable platform (output), coarse actuator inputs, and fine actuator inputs, respectively.

### *3.1. Required fine actuator strokes*

To realize continuous fine positioning, the strokes of the fine actuators should be larger than the resolutions of the coarse actuators. The resolutions of the coarse actuators can be written in Eq. (8) from the specifications of the selected coarse actuators in Fig. 6.

$$\Delta \rho_{C,resolution} = \begin{Bmatrix} \Delta Z_{C1,resolution} \\ \Delta Z_{C2,resolution} \\ \Delta Z_{C3,resolution} \end{Bmatrix} = \begin{Bmatrix} 0.250\,\mu m \\ 0.250\,\mu m \\ 0.016\,\mu m \end{Bmatrix} \quad (8)$$

From Eq. (8) and Table II, the required $Z_{f1}$, $Z_{f2}$ and $Z_{f3}$ fine actuator stroke distributions within workspace are calculated and displayed in Fig. 16 and Fig. 17. The required strokes of $Z_{f1}$ and $Z_{f2}$ fine actuators should be larger than 0.250 μm, 0.455 μm, and 0.219 μm for the vertical types (VV and VH types), horizontal types (HV and HH types), and variable link types (NV and NH types), respectively, as shown in Fig. 16 where the minus signs for the $Z_{f2}$ fine actuator of the horizontal types (HV, HH) mean that the fine actuator moves in the opposite direction of the coarse actuator. These results indicate that the required strokes of $Z_{f1}$ and $Z_{f2}$ fine actuators should be 1.0000 times (= 0.250 μm/0.250 μm), 1.8200 times (= 0.455 μm/0.250 μm), and 0.8760 times (= 0.219 μm/0.250 μm) larger than the resolutions of the coarse actuators for the vertical types (VV and VH types), horizontal types (HV and HH types), and variable link types (NV and NH types), respectively.

In case of $Z_{f3}$ fine actuator, the required strokes should be larger than 0.0160 μm and 0.0195 μm for the vertical types (VV, HV, and NV types) and horizontal types (VH, HH, and NH types), respectively, as shown in Fig. 17. These results mean that the required strokes of the $Z_{f3}$ fine actuator should

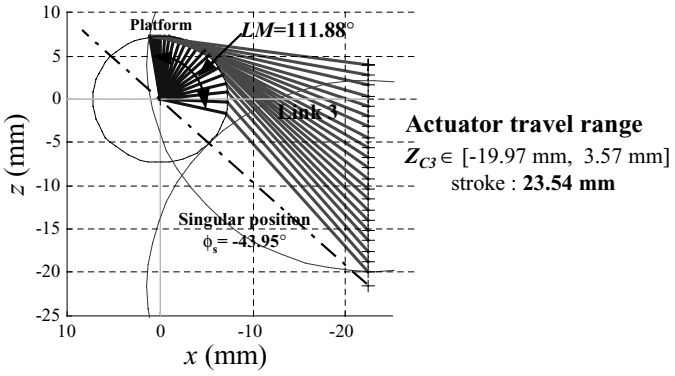


Fig. 13. Local mobility at $O'(0,0,0)$ considering the $Z_{c3}$ actuator travel range.

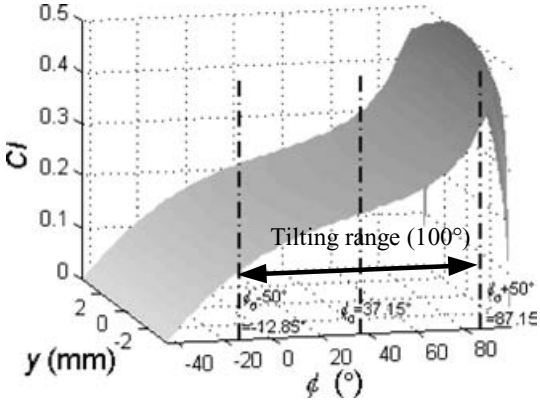


Fig. 14. Conditioning index (*CI*) distribution.

https://doi.org/10.1017/S0263574704000402 Published online by Cambridge University Press

Table II. Equations for evaluating each fine actuator architecture.

| F-Type | Jacobian for dual stage | Fine actuator stroke | Platform resolution |
|---|---|---|---|
| VV | $\Delta \boldsymbol{p} = \boldsymbol{J}_{VV}^{-1}(\Delta \boldsymbol{\rho}_C + \Delta \boldsymbol{\rho}_F)$ | $\Delta \boldsymbol{\rho}_{F,stroke} \geq \Delta \boldsymbol{\rho}_{C,resolution}$ | $\Delta \boldsymbol{p}_{resolution} = \boldsymbol{J}_{VV}^{-1} \Delta \boldsymbol{\rho}_{F,resolution}$ |
| VH | $\Delta \boldsymbol{p} = \boldsymbol{J}_{VV}^{-1} \Delta \boldsymbol{\rho}_C + \boldsymbol{J}_{VH}^{-1} \Delta \boldsymbol{\rho}_F$ | $\Delta \boldsymbol{\rho}_{F,stroke} \geq (\boldsymbol{J}_{VH} \boldsymbol{J}_{VV}^{-1}) \Delta \boldsymbol{\rho}_{C,resolution}$ | $\Delta \boldsymbol{p}_{resolution} = \boldsymbol{J}_{VH}^{-1} \Delta \boldsymbol{\rho}_{F,resolution}$ |
| HV | $\Delta \boldsymbol{p} = \boldsymbol{J}_{VV}^{-1} \Delta \boldsymbol{\rho}_C + \boldsymbol{J}_{HV}^{-1} \Delta \boldsymbol{\rho}_F$ | $\Delta \boldsymbol{\rho}_{F,stroke} \geq (\boldsymbol{J}_{HV} \boldsymbol{J}_{VV}^{-1}) \Delta \boldsymbol{\rho}_{C,resolution}$ | $\Delta \boldsymbol{p}_{resolution} = \boldsymbol{J}_{HV}^{-1} \Delta \boldsymbol{\rho}_{F,resolution}$ |
| HH | $\Delta \boldsymbol{p} = \boldsymbol{J}_{VV}^{-1} \Delta \boldsymbol{\rho}_C + \boldsymbol{J}_{HH}^{-1} \Delta \boldsymbol{\rho}_F$ | $\Delta \boldsymbol{\rho}_{F,stroke} \geq (\boldsymbol{J}_{HH} \boldsymbol{J}_{VV}^{-1}) \Delta \boldsymbol{\rho}_{C,resolution}$ | $\Delta \boldsymbol{p}_{resolution} = \boldsymbol{J}_{HH}^{-1} \Delta \boldsymbol{\rho}_{F,resolution}$ |
| NV | $\Delta \boldsymbol{p} = \boldsymbol{J}_{VV}^{-1} \Delta \boldsymbol{\rho}_C + \boldsymbol{J}_{NV}^{-1} \Delta \boldsymbol{\rho}_F$ | $\Delta \boldsymbol{\rho}_{F,stroke} \geq (\boldsymbol{J}_{NV} \boldsymbol{J}_{VV}^{-1}) \Delta \boldsymbol{\rho}_{C,resolution}$ | $\Delta \boldsymbol{p}_{resolution} = \boldsymbol{J}_{NV}^{-1} \Delta \boldsymbol{\rho}_{F,resolution}$ |
| NH | $\Delta \boldsymbol{p} = \boldsymbol{J}_{VV}^{-1} \Delta \boldsymbol{\rho}_C + \boldsymbol{J}_{NH}^{-1} \Delta \boldsymbol{\rho}_F$ | $\Delta \boldsymbol{\rho}_{F,stroke} \geq (\boldsymbol{J}_{NH} \boldsymbol{J}_{VV}^{-1}) \Delta \boldsymbol{\rho}_{C,resolution}$ | $\Delta \boldsymbol{p}_{resolution} = \boldsymbol{J}_{NH}^{-1} \Delta \boldsymbol{\rho}_{F,resolution}$ |

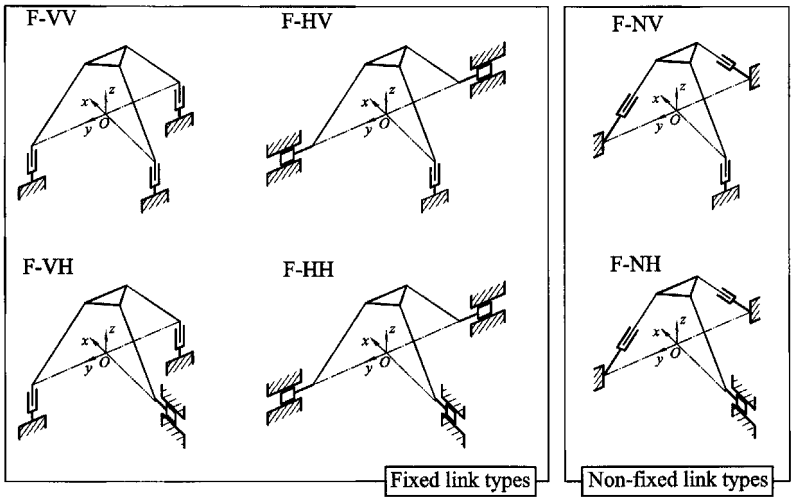


Fig. 15. Six possible architectures with fine actuators.

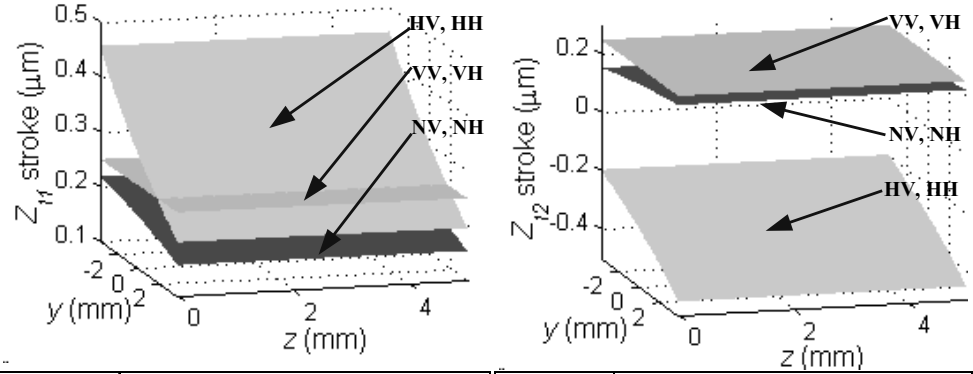


| Type | $Z_{f1}$ fine actuator stroke(μm) | | |
|---|---|---|---|
| | max | min | average |
| VV,VH | **0.250** | 0.250 | 0.250 |
| HV,HH | **0.455** | 0.196 | 0.312 |
| NV,NH | **0.219** | 0.154 | 0.191 |

(a) $Z_{f1}$ stroke distribution

| Type | $Z_{f2}$ fine actuator stroke(μm) | | |
|---|---|---|---|
| | max | min | average |
| VV,VH | **0.250** | 0.250 | 0.250 |
| HV,HH | -0.196 | **-0.455** | -0.311 |
| NV,NH | **0.219** | 0.154 | 0.191 |

(b) $Z_{f2}$ stroke distribution

Fig. 16. Required $Z_{f1}$ and $Z_{f2}$ fine actuator stroke distributions within the workspace.

be 1.0000 times (= 0.0160 μm/0.0160 μm) and 1.2190 times (= 0.0195 μm/0.0160 μm) larger than the resolutions of the coarse actuators for the vertical types (VV, HV, and NV types) and horizontal types(VH, HH, and NH types), respectively.

Above results are summarized in Table III, which can be used for selecting fine actuators in terms of the required stroke. Especially, the ratio of the required fine actuator stroke to the coarse actuator resolutions in Table III(b) can be useful in calculating the required fine actuator strokes with respect to the other types of coarse actuators having different resolutions for the optimal parameter set of the mechanism in Fig. 10.

https://doi.org/10.1017/S0263574704000402 Published online by Cambridge University Press

Table III. Summary of the required fine actuator strokes for each type.

(a) Required strokes (unit: μm)

| Type | $Z_{f1}$ | $Z_{f2}$ | $Z_{f3}$ |
|---|---|---|---|
| VV | 0.2500 | 0.2500 | 0.0160 |
| VH | 0.2500 | 0.2500 | 0.0195 |
| HV | 0.4550 | −0.4550 | 0.0160 |
| HH | 0.4550 | −0.4550 | 0.0195 |
| NV | 0.2190 | 0.2190 | 0.0160 |
| NH | 0.2190 | 0.2190 | 0.0195 |

(b) Ratio of fine actuator strokes to coarse actuator resolutions

| Type | $Z_{f1}$ | $Z_{f2}$ | $Z_{f3}$ |
|---|---|---|---|
| VV | 1.0000 | 1.0000 | 1.0000 |
| VH | 1.0000 | 1.0000 | 1.2190 |
| HV | 1.8210 | −1.8210 | 1.0000 |
| HH | 1.8210 | −1.8210 | 1.2190 |
| NV | 0.8760 | 0.8760 | 1.0000 |
| NH | 0.8760 | 0.8760 | 1.2190 |

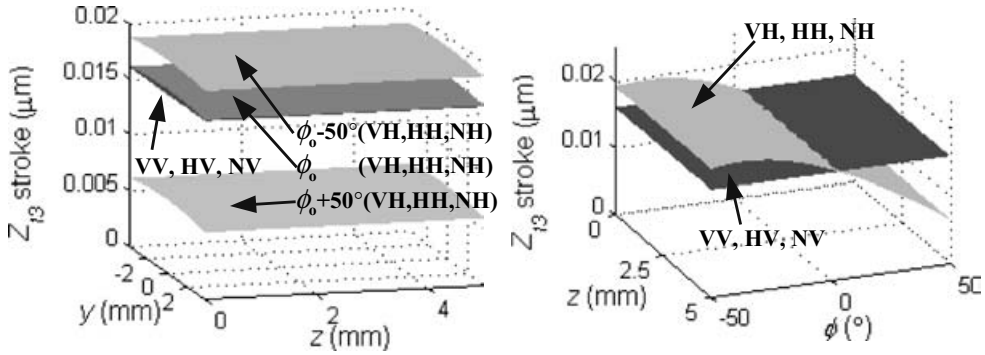


| Type | $Z_{f3}$ fine actuator stroke(μm) | | |
|---|---|---|---|
| | max | min | average |
| VV,HV,NV | **0.0160** | 0.0160 | 0.0160 |
| VH,HH,NH | **0.0191** | 0.0060 | 0.0139 |

(a) $Z_{f3}$ stroke distribution

| Type | $Z_{f3}$ fine actuator stroke(μm) | | |
|---|---|---|---|
| | max | min | average |
| VV,HV,NV | **0.0160** | 0.0160 | 0.0160 |
| VH,HH,NH | **0.0195** | 0.0066 | 0.0153 |

(b) $Z_{f3}$ stroke distribution at $y$=0

Fig. 17. Required $Z_{f3}$ fine actuator stroke distribution within the workspace.

### *3.2. Platform resolution analysis*

There are three basic definitions with respect to how well a machine can position its axes: resolution, repeatability, and accuracy.[6] Resolution is the larger of the smallest programmable step or the smallest step a machine can make during point-to-point motion. Repeatability is the error between a number of successive attempts to move the machine to the same position. Accuracy is the maximum translational or rotational error between any two points in the machine's workspace as a result of the imperfections in the machine. Accuracy represents the maximum difference between the commanded (ideal) position and the actual position for any given input, which is affected by a combination of a number of terms representing uncertainty in the measurement and calibration process such as backlash, hysteresis, drift, nonlinearity and repeatability. Therefore, accuracy cannot be better than repeatability, and can be much worse. And, resolution is important because it gives a lower bound on the repeatability that a machine could obtain if one really tried. Usually the accuracy of a machine is five to ten times worse than the resolution.[7]

In this sense, the platform resolution of the micro mechanism should be as small as possible to achieve better accuracy. Hence, it is desirable to attain smaller resolution in the selection problem of the fine actuator architecture. Platform resolutions can be calculated in terms of the fine actuator resolutions by the equations of the fourth column in Table II.

The platform resolution can be evaluated by assuming unit movements of the $Z_{f1}$ and $Z_{f3}$ fine actuators independently. As shown in the example of the evaluation method for the VV type fine actuator architecture of Fig. 18, the unit movement of the $Z_{f1}$ fine actuator makes the $y$, $z$, and $\phi$ directional combined motions while the unit movement of $Z_{f3}$ fine actuator only makes the $\phi$ directional motion. Hence, the $y$ and $z$ directional resolutions of the platform can be evaluated by the unit movement of the $Z_{f1}$ fine actuator and the $\phi$ directional resolutions of the platform can be evaluated by the unit movement of the $Z_{f3}$ fine actuator for the six possible fine actuator architectures.

The results of calculating the $y$ and $z$ directional resolutions within the workspace for each fine actuator architecture are shown in Fig. 19, where the average resolutions of the horizontal types (HV and HH types) in the 1st and 2nd legs are smaller than those of other types. Thus the horizontal types (HV and HH types) in the 1st and 2nd legs can be selected for the fine actuator architecture.

Figure 20 shows the distributions of the $\phi$ directional resolutions by the unit movement of the $Z_{f3}$ fine actuators for each fine actuator architecture at $y = 0$ mm and $y = \pm\frac{R_1}{2} = \pm 3.66$ mm. The vertical types in the 3rd leg (VV, HV, and NV types) and horizontal types in 3rd leg (VH, HH, and NH

https://doi.org/10.1017/S0263574704000402 Published online by Cambridge University Press

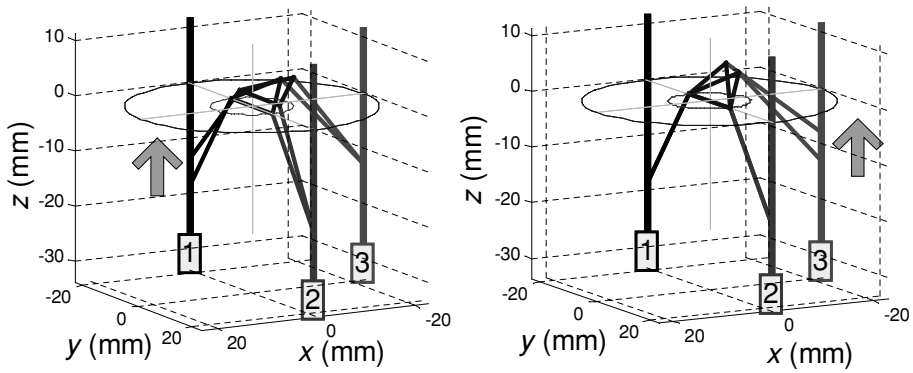


(a) Unit movement of the $Z_{f1}$ actuator ($y$, $z$) (b) Unit movement of the $Z_{f3}$ actuator ($\phi$)

Fig. 18. Evaluation method for the platform resolution (VV type fine actuator architecture).

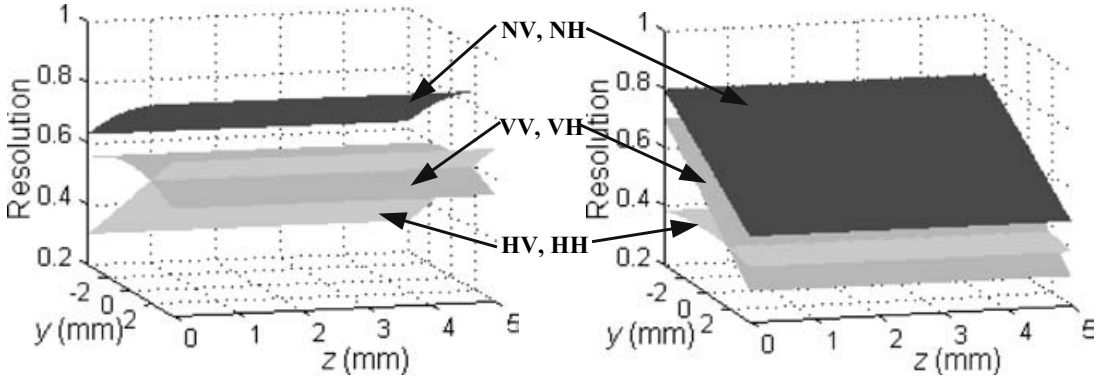


| Type | $y$ direction platform resolution | | |
|---|---|---|---|
| | max | min | average |
| VV, VH | 0.6093 | 0.5476 | 0.5886 |
| HV, HH | **0.6992** | **0.3008** | **0.5000** |
| NV, NH | 0.8881 | 0.6248 | 0.7775 |

(a) $y$ directional resolution

| Type | $z$ direction platform resolution | | |
|---|---|---|---|
| | max | min | average |
| VV, VH | 0.6992 | 0.3008 | 0.5000 |
| HV, HH | **0.4103** | **0.3840** | **0.4013** |
| NV, NH | 0.7978 | 0.4878 | 0.6454 |

(b) $z$ directional resolution

Fig. 19. Distributions of the $y$ & $z$ directional resolutions by the unit movement of the $Z_{f1}$ fine actuator.

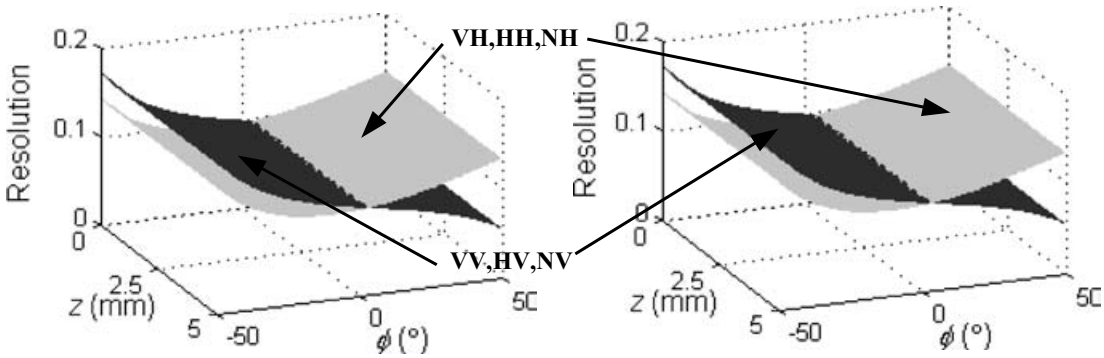


| Type | $\phi$ direction platform resolution | | | |
|---|---|---|---|---|
| | max | min | average | standard dev. |
| VV, HV, NV | 0.1732 | 0.0551 | 0.1027 | 0.0274 |
| VH, HH, NH | 0.1451 | 0.0944 | 0.1091 | **0.0134** |

(a) $\phi$ directional resolution at $y$=0 mm

| Type | $\phi$ direction platform resolution | | | |
|---|---|---|---|---|
| | max | min | average | standard dev. |
| VV, HV, NV | 0.1741 | 0.0505 | 0.1015 | 0.0285 |
| VH, HH, NH | 0.1487 | 0.0958 | 0.1105 | **0.0135** |

(b) $\phi$ directional resolution at $y$=±3.66 mm

Fig. 20. Distributions of the $\phi$ directional resolutions by the unit movement of the $Z_{f3}$ fine actuator.

https://doi.org/10.1017/S0263574704000402 Published online by Cambridge University Press

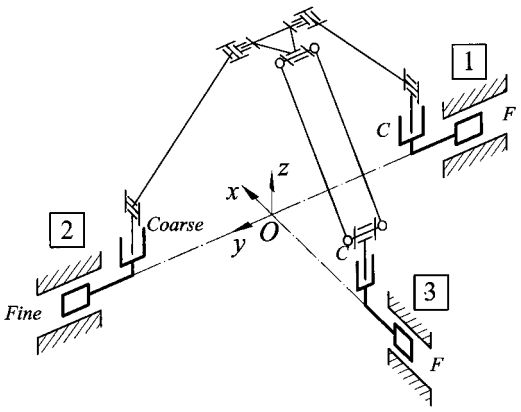


Fig. 21. Selected coarse-and-fine actuator combination (C-VV: F-HH).

types) have similar average resolutions but the horizontal types in the 3rd leg have less variation than the vertical types judging from the graph shapes and the calculated standard deviations. Thus the horizontal types in the 3rd leg (VH, HH, and NH types) can be selected for the fine actuator architecture.

From these results of Fig. 19 and Fig. 20, we can conclude that the horizontal types have smaller platform resolutions for both the 1st/2nd legs and the 3rd leg in the fine actuator architecture. So the F-HH type can be selected for the fine actuator architecture. Recalling the selection of the C-VV type for the coarse actuator architecture in part I, the final selected coarse-and-fine actuator combination is C-VV: F-HH as shown in Fig. 21.

Based on the analysis of the required fine actuator stroke and the platform resolution, the commercial translation piezoelectric stages of Table IV are selected for the three fine actuators of our mechanism. Each one has the stroke of 32 μm with closed loop control, which is enough for the HH type stroke requirement of more than 0.455 μm as shown in Table III(a). And they have 0.05 nm resolution, which lead to the theoretical $y$ directional resolutions from 0.01052 nm to 0.03496 nm, the theoretical $z$ directional resolutions from 0.00788 nm to 0.02052 nm, and the theoretical $\phi$ directional resolution from 0.00070 radian to 0.00744 radian as shown in Table V.

## 4. DESIGN OF A MICRO POSITIONING PLATFORM

In former sections, to achieve sub-micro precision positioning with a large working space, the 3-DOF micro parallel mechanism with the dual stage system is introduced. The C-VV type for the coarse actuator architecture and the F-HH type for the fine actuator architecture are selected for the micro parallel mechanism with the dual stage system.

To be applied for the sub-micro precision positioning, the joints of the mechanism should have little or no friction and backlash. Usually a flexure joint is used for precision positioning.[8,9] A flexure is a frictionless, stictionless linkage based on the elastic deformation (flexing) of a solid material. Sliding and rolling are eliminated. In addition to absence of internal friction, flexure devices exhibit zero backlash, no lubrication, smooth motion, virtually-infinite resolution, high stiffness and load capacity, and resistance to shock and vibration. However, the accuracy of a flexure hinge is often difficult to attain due to shape change and residual stress caused by mechanical machining process. While simple in shape and operation flexures are mathematically complex and need time-consuming numerical procedures such as FEM analysis. And because the most usual flexure joints allow only small strokes, it only provide short-range motion, which is not suitable for some applications such as high accuracy motion with large motion range. Therefore flexure hinges cannot be used for the micro parallel positioning platform with the dual stage system.

Currently we are also developing the joints for the micro parallel mechanism. To apply for the mechanism, we need one DOF and two DOF joints. The concept of these two joints is shown in Fig. 22. It is a kind of rocking joint turning around the center globe. Because the center globe is assembled under pre-load, it is capable of smooth rocking motion with very low frictional resistance and zero clearance. It can promise extra-high performance with respect to precision and rigidity in the allowable moving range.

The micro parallel mechanism will be used for the micro positioning platform that is being developed at Robust Design Engineering Laboratory in Seoul National University. The embodiment design of the 3-DOF micro positioning platform with the dual stage is shown in Fig. 23(a). For the coarse actuators, three miniaturized linear actuators of Fig. 7 will be used to offer a large working space. For the fine

Table IV. Detail specifications of the fine actuator to be used.

| Items | Specifications of the fine actuator | Figure |
|---|---|---|
| Stroke | 38/32 μm (open/closed loop) |  |
| Max. load | 100 N (force generation 30 N) | |
| Resolution | 0.05 nm | |
| Accuracy | 30 nm (typ. Repeatability), 46 nm (typ. Non linearity) | |
| Dimension | 40 × 40 × 25 mm | |
| Weight | 77 g | |
| Operating voltage | −10 ∼ 150 V | |
| Position feedback | O (strain gauges) | |
| Stiffness | 1 N/μm | |
| Resonant freq. | 760 Hz | |



https://doi.org/10.1017/S0263574704000402 Published online by Cambridge University Press

Table V. Theoretical platform resolutions based on the selected fine actuators.

| | Rate | | | Theoretic platform resolution | |
|---|---|---|---|---|---|
| Axis | max | min | Fine actuator Resolution (nm) | max | min |
| $y$ | 0.6992 | 0.3008 | 0.05 nm | **0.03496 nm** | 0.01052 nm |
| $z$ | 0.4103 | 0.3840 | 0.05 nm | **0.02052 nm** | 0.00788 nm |
| $\phi$ | 0.1487 | 0.0944 | 0.05 nm | **0.00744 rad.** | 0.00070 rad. |

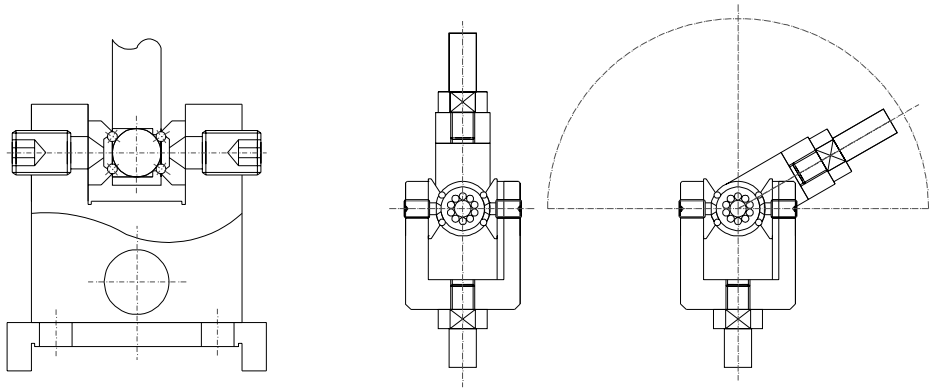

(a) one DOF joint (b) two DOF joint

Fig. 22. Concept for the joints to be used in the mechanism.

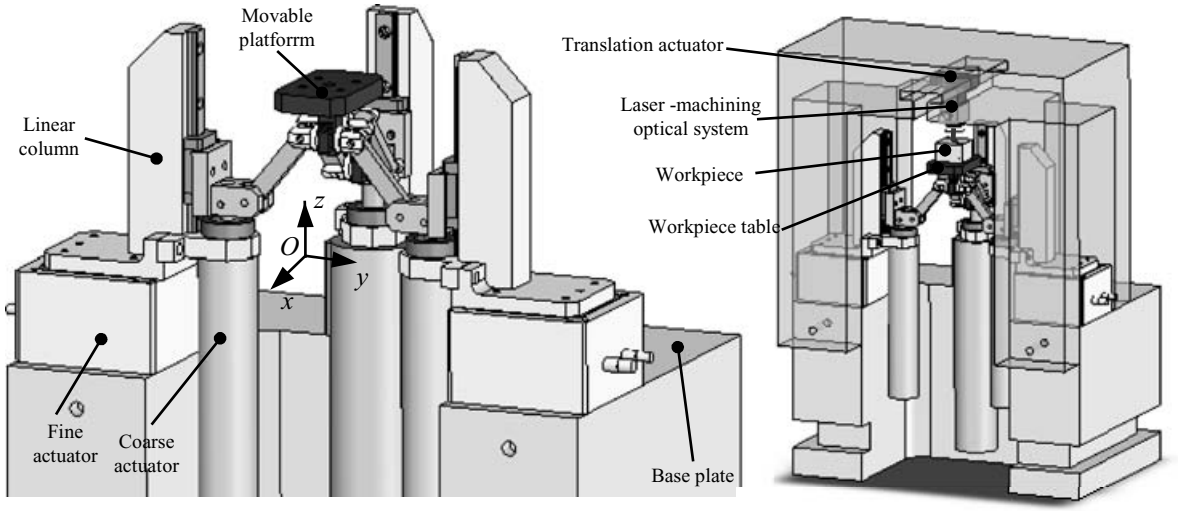


(a) Basic micro positioning platform with the dual stage. (b) Laser-machining application

Fig. 23. Three-dimensional model for the micro positioning platform.

actuators, three translation piezoelectric stages of Table IV will be used to enable smaller platform resolution of the motion supporting the whole mechanism. The workspace is 5 mm ($y$-axis) × 5 mm ($z$-axis). The basic size of the micro positioning platform is 45.0 mm × 22.5 mm × 22.9 mm, excluding the machining device and actuators. Assuming that the kinematic parameter set is perfect without errors, the theoretic platform resolution of the micro positioning platform is about 0.01 ∼ 0.04 nm due to the precise fine actuator with 0.05 nm resolution as shown in Table V.

The three-dimensional model of the micro positioning platform for laser-machining application is shown in Fig. 23(b). A workpiece table is arranged on the moving platform and a laser-machining optical system is arranged above the workpiece table. A translation actuator to drive the laser-machining optical system along the $x$-axis is embedded in the upper laser-machining optical system. Thus, the machine has four DOFs, where the workpiece table can conduct a movement of three DOFs by virtue of the parallel mechanism, and the laser machining optical system can conduct a movement of one translational DOF along $x$-axis. By adding the laser-machining device on top of the micro positioning platform as shown in Fig. 23(b), this machine with 100° mobility will be used to make three dimensional micro

https://doi.org/10.1017/S0263574704000402 Published online by Cambridge University Press

mechanical components whose lengths are from 0.01 mm to 5 mm with sub-micro accuracy.

## 5. CONCLUSIONS

An optimal kinematic parameter set is determined for the selected coarse actuator architecture of the proposed three degree-of-freedom miniaturized micro parallel mechanism with high mobility, high accuracy, and a large working space by using the dual stage system. A design tool, the physical model of the solution space, is used for this design optimization based on the performance evaluation of the conditioning index (*CI*) and global mobility conditioning index (*GMCI*). Here, the different design aspects in the micro machine design such as previous consideration of available coarse actuators before the real design process, manufacturability, and easy assembly are addressed. The selected optimal kinematic parameter set is $R_1 = 7.32$ mm, $R_2 = 18.50$ mm, $R_3 = 22.50$ mm, $L = 23.93$ mm and $\phi_o = 37.15^\circ$, where the basic size of the micro parallel mechanism, excluding the actuators, is 45.0 mm × 22.5 mm × 22.9 mm with 100° mobility and workspace of 5 mm ($y$-axis) × 5 mm ($z$-axis).

After finishing the design of the main coarse actuator architecture, the F-HH type fine actuator architecture among the six possible fine actuator architectures is selected to achieve sub micron positioning accuracy based on the requirements of the continuous fine motion and smaller platform resolution. Finally, the design application for the micro positioning platform based on the selected coarse and fine actuator combination is presented.

**Acknowledgement**

This work was supported by the NRL Program on Next Generation Parallel Mechanism Platforms and partly by the Micro-thermal System ERC and the Brain Korea 21 Project in 2003.

## References

1. P. Y. Papalambros and D. J. Wilde, *Principles of Optimal design: Modeling and Computation*, 2nd ed. (Cambridge University Press, Cambridge, UK, 2000).
2. *Optimization Toolbox User's Guide* (The MathWorks, Inc., 2002).
3. X.-J. Liu, J. Wang, F. Gao and L.-P. Wang, "Mechanism design of a simplified 6-DOF 6-RUS parallel manipulator," *Robotica* **20**(1), 81–91 (2002).
4. S. H. Chang, C. K. Tseng and H. C. Chien, "An Ultra-Precision XYQz Piezo-Micropositioner Part I: Design and analysis," *IEEE Transactions on Ultrasonics, Ferroelectrics, and Frequency Control* **46**(4), 897–905 (1999).
5. Y. Takeda, K. Ichikawa, H. Funabashi and K. Hirose, "An In-Parallel Actuated Manipulator with Redundant Actuators for Gross and Fine Motions," *Proceedings of the 2003 IEEE International Conference on Robotics & Automation*, Taipei, Taiwan (September 14–19, 2003) pp. 749–754.
6. A. H. Slocum, *Precision Machine Design* (Prentice-Hall, Inc., New Jersey, USA, 1992) pp. 58–60.
7. H. Nakazawa, *Principles of Precision Engineering* (Oxford university press, New York, USA, 1994) pp. 14–32.
8. N. Lobontiu, J. S. N. Paine, E. O'Malley and M. Samuelson, "Parablic and Hyperbolic flexure hignes: flexibility, motion precision and stress characterization based on compliance closed-form equations," *Precision Engineering* **26**, 183–192 (2002).
9. J. E. McInroy and J. C. Hamann, "Design and Control of Flexure Jointed Hexapods," *IEEE Transactions on Robotics and Automation* **16**(4), 372–381 (2000).

https://doi.org/10.1017/S0263574704000402 Published online by Cambridge University Press